Chapter 4

Sources and Data

This chapter serves two purposes. Firstly, we introduce the Parkes Half-Jansky Flat-spectrum Sample, a catalogue comprising 323 radio-loud flat-spectrum objects first published by Drinkwater et al. (1997). This catalogue forms the basis for the modelling and analysis that will be done in this thesis. Secondly, we present the optical photometry that will be used in the actual modelling. This data has already been published (Francis, Whiting, and Webster 2000), but it is presented here also, together with additions and alterations specific to the modelling performed later in the thesis.

Additionally, a note for completeness: whenever names of sources from the sample are presented in this thesis, they are specified in the standard form HHMM±DDD, where "HHMM" is the right ascension of the source in hours and minutes, and "DDD" is the declination to the nearest tenth of a degree. Both right ascension and declination are in B1950 coordinates. In the literature, sources from the Parkes Catalogue (as all these sources are) have the prefix "PKS". For the purposes of brevity, however, this has been omitted from all the source names for the remainder of this thesis.

4.1 The Sample

During the 1960s and 1970s, the 64m radio telescope near Parkes in New South Wales surveyed the entire sky (as visible from the telescope) at 2.7 GHz, generating a catalogue that numbered nearly 11,000 sources. Many of these sources are AGN or quasars, and so this catalogue represents a huge resource of possible candidates for radio-selected quasars.

This was taken advantage of in the creation of the Parkes Half-Jansky Flat-Spectrum Sample (hereafter PHFS) (Drinkwater et al. 1997). This is a sample of bright radio sources, taken from the machine-readable version of the Parkes Catalogue (PKSCAT90, Wright and Otrupcek 1990), that have a flat radio spectrum based on the fluxes from the catalogue. The criteria for selection are:

Observed:	Fluxes at both 5.0 GHz and 2.7 GHz exist in the Parkes Catalogue (PKSCAT90).
Radio loud:	$S_{2.7\mathrm{GHz}} > 0.5$Jy
Flat spectrum:	Radio spectral index $\alpha_{2.7/5.0} > -0.5$, where $S_\nu \propto \nu^\alpha$.
Position:	Galactic latitude: $\|b\| > 20°$
Position:	Declination (B1950.0): $-45° < \delta < +10°$

Note that the spectral index is derived from the 2.7 and 5 GHz fluxes from the catalogue. However, these fluxes were taken at different times – sometimes up to more than a year apart – and so, if the source in question had varied in flux between these observations, this spectral index will not be the true radio continuum slope of the quasar. More recent contemporaneous observations[1] using the Australia Telescope Compact Array, have shown that $\sim 10\%$ of the sources are incorrectly included in the PHFS (a greater number than predicted by Drinkwater et al. (1997)), as their true radio spectral index is steeper than -0.5. Additionally, a similar number will have been excluded for having an apparently steep index.

The Galactic latitude requirement was included to exclude those sources close to the Galactic plane, where increased optical extinction by dust, as well as the increased density of sources, would pose a problem in the identification and study of the optical counterparts of the sources. The declination limits were imposed purely to limit the size of the sample. These criteria resulted in a total of 323 sources.

The resulting sample of radio sources is quite heterogeneous. The sources included range from low redshift radio galaxies (including narrow-line radio galaxies and steep (radio) spectrum galaxies), through the spectrum of traditional quasars – both optically bright and optically faint – with a number

[1]These observations are currently ongoing, and have involved many people at the University of Melbourne.

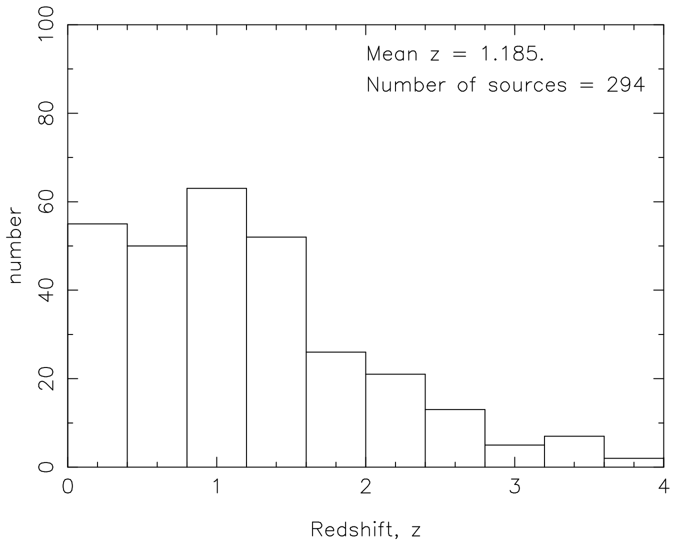

Figure 4.1: Distribution of redshifts for sources from the PHFS.

of BL Lac objects, up to some very high redshift quasars. The redshift distribution for those sources with measured redshift (a total of 294 sources out of 323) is shown in Fig. 4.1. The 29 sources that do not have a measured redshift generally fall into two distinct classes: BL Lac objects, with no measurable emission lines from which to deduce the redshift; or optically faint sources that are too faint to get a suitable spectrum from which to measure a redshift.

While the radio properties of the objects are all very similar (by virtue of the selection process), the optical properties vary considerably. The most obvious effect, first pointed out by Webster et al. (1995), is that there is a very large dispersion in their $B-K$ colours (that is, the ratio of flux in the K band (infrared: 2.2μm) to the B band (blue: 0.4μm)). This range, $2 < B-K < 8$, is much greater than that seen in typical optically-selected samples of quasars (for instance, the Large Bright Quasar Survey, or LBQS, has a range of $2 \lesssim B-K \lesssim 4$).

Webster et al. interpreted this range of optical-NIR colours as being due to the presence of large amounts of dust, that obscures the quasar at optical wavelengths. This had the implication that, if similar amounts of dust were present in radio-quiet quasars (as suggested by X-ray observations), then optical surveys of bright quasars may be missing up to 80% of quasars for a given intrinsic magnitude.

Serjeant and Rawlings (1996), however, suggested the alternative interpretation that the red optical colours are due to the presence of a red, optical synchrotron component. This component would likely be an extension of the beamed radio emission. This idea will be tested by the modelling in Chapter 5.

Finally, we note that a further alternative explanation was offered by Benn et al. (1998). They investigated a sample of radio-selected quasars (the B3-VLA quasar sample, Vigotti et al. (1997)), and found that many of them exhibited an excess of light in the K band. They argued that this light mostly came from star-light from the host galaxy. The B3 sample is dominated by steep radio-spectrum sources, and, according to unified schemes, the central AGN source should be subject to more obscuration than for flat-spectrum sources, making it easier to detect the galactic emission. This explanation, however, was tested by Masci et al. (1998), and rejected as an explanation for the spread in optical colours of the PHFS sources.

4.2 Observational data

To attempt to solve the puzzle of the red optical-NIR colours, it was decided to make observations of the PHFS quasars at seven wave-bands, covering the optical and NIR wavelength ranges: B ($\lambda \sim 0.44\mu$m), V ($\lambda \sim 0.55\mu$m), R ($\lambda \sim 0.7\mu$m), I ($\lambda \sim 0.88\mu$m), J ($\lambda \sim 1.24\mu$m), H ($\lambda \sim 1.65\mu$m), and K ($\lambda \sim 2.19\mu$m). Having this many data points in the optical and NIR range of the spectrum makes it far easier to accurately model the spectral energy distributions (SEDs) of the Parkes quasars, and hopefully determine the nature of the reddening mechanism. The results of these observations have been published by Francis et al. (2000). However the method and results of observations are discussed here, as well as the choice of data that is used in this thesis.

4.3 The new observations

Over the course of 26 nights in 1997, a total of 157 sources from the PHFS were observed, using the Australian National University's 1 metre[2] and 2.3

[2] Or, as it is traditionally known, the "40 inch".

metre telescopes. The optical observations were made using either the 1m or the imager on the 2.3m telescope, while the NIR observations were made with the *CASPIR* 256×256 InSb array camera (McGregor et al. 1994) on the 2.3m telescope. The methods of the observations and data reduction are explained in detail in Francis et al. (2000), so they will not be repeated here.

To minimise the effects of variability, the optical and NIR observations for each object were made as close as possible in time to each other (the largest spread in time for a single object was six nights, and most sources had a spread much shorter than this).

It should be noted that variability has been seen on timescales less than this. So-called "intra-day variability" (IDV) has been commonly seen at radio frequencies in many radio loud quasars, including many of the objects observed here (see, for example Kedziora-Chudczer (1998), or the review of IDV properties by Wagner and Witzel (1995)). Such variability has also been seen at optical and NIR wavelengths (Heidt and Wagner 1996; Romero, Cellone, and Combi 1999), mainly in sources such as BL Lac objects and flat-spectrum radio quasars (i.e. the sort of object found in the PHFS). While the radio variations could be due to scintillation of an intrinsically small source by the interstellar medium, this cannot explain the variability at infrared and optical frequencies. Instead, these variations are thought to be due to relativistic shocks propagating down jets, or the interactions of these shocks with features in the jets. This model is preferred to one where the variations are due to flares or hot spots on the accretion disk, primarily because of the low incidence of optical intra-day variability seen in radio-quiet quasars (which either have very weak jets or are without them) (Jang and Miller 1997; Romero et al. 1999). However, see Chapter 8 for a result that challenges this. Amplitudes of this variation can be up to 0.1 magnitudes over the course of one night.

For the purposes of modelling and plotting the data, the magnitudes need to be converted into fluxes. The assumed fluxes for objects of zero magnitude are listed in Table 4.1. In the optical, the filter sets used approximate the Johnson & Cousins system (the calibration was done using Graham standards, which also approximate this system), and the zero magnitude fluxes are taken from Bessell, Castelli, and Plez (1998). The NIR observations were made using the *CASPIR* filter set, calibrated with *IRIS* standards, and the

Band	Mean λ (μm)	Zero magnitude flux (F_λ, W m^{-2} μm^{-1})
B	0.440	6.32×10^{-8}
V	0.550	3.63×10^{-8}
R	0.700	2.18×10^{-8}
I	0.880	1.13×10^{-8}
J	1.239	3.11×10^{-9}
H	1.649	1.15×10^{-9}
K	2.192	4.10×10^{-10}

Table 4.1: Assumed fluxes of a star with zero magnitude, for each of the wave-bands used.

zero magnitude fluxes used are those calculated by P. McGregor[3] assuming that the star Vega is well represented in the NIR by a black body of temperature 11200 K and normalisation $F_\lambda(555\text{nm}) = 3.44 \times 10^{-12}$ W cm^{-2} μm^{-1} (Bersanelli, Bouchet, and Falomo 1991). The observations were made with the *CASPIR* K_n filter, but were calibrated using the K magnitudes of the *IRIS* system without a colour correction term applied. They have thus been normalised using a K-band zero point (Table 4.1).

4.4 Photometry

The photometry confirms the result presented in Webster et al. (1995), namely that there is a large spread in $B-K$ colours in the PHFS quasars. This distribution is shown in Fig. 4.2, along with the distribution of colours for a small representative sample of quasars from the LBQS. As can be clearly seen, the PHFS distribution is much broader and contains many quite red objects. Also note that the lower envelope of the PHFS distribution is approximately the same as that of the LBQS quasars – i.e. there are not really any sources in the PHFS that are significantly bluer than the optically selected quasars. (The one outlying source in Fig. 4.2 is 0232−042, which has a very blue SED: $B-K = 1.45$.)

In Fig. 4.3 is plotted a histogram of the absolute magnitudes of the PHFS sources with simultaneous photometry. The absolute magnitude is

[3]CASPIR manual, Mount Stromlo & Siding Spring Observatories, Australian National University. http://msowww.anu.edu.au/observing/teldocs/2.3m/CASPIR/

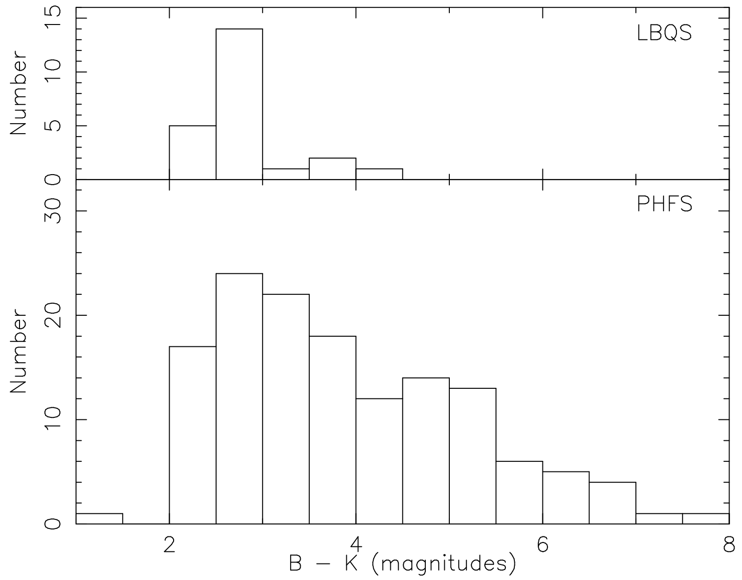

Figure 4.2: Distribution of $B - K$ colours for the PHFS sources with quasi-simultaneous photometry. The top panel shows a small representative sample of sources from the LBQS – the photometry is taken from Francis (1996) and Francis et al. (2000).

calculated by

$$M_V = m_V - 5\log_{10}(d_L) + 2.5(1+\alpha)\log_{10}(1+z) - 25 \qquad (4.1)$$

where m_V is the apparent V magnitude, d_L is the luminosity distance, in Mpc, to redshift z, and α is the spectral index ($F_\nu \propto \nu^\alpha$). In calculating M_V, we used the best-fit spectral index to the optical photometry (that is, B, V, R, and I magnitudes). The term $K(z) = -2.5(1+\alpha)\log_{10}(1+z)$ is the K-correction term (Peterson 1997).

One can use the absolute magnitude to discriminate between sources of quasar and Seyfert luminosity. The dividing line is traditionally given by

$$M_V = -21.5 + 5\log_{10} h \qquad (4.2)$$

where $H_0 = 100h$ km s^{-1} Mpc^{-1}. As can be seen in Fig. 4.3, there are 16 sources in this sub-sample of the PHFS that are of Seyfert luminosity. These sources are either low-redshift galaxies, or optically faint sources (that are not necessarily at a low redshift). We note that the distribution from quasar to Seyfert luminosities is continuous, demonstrating that the division

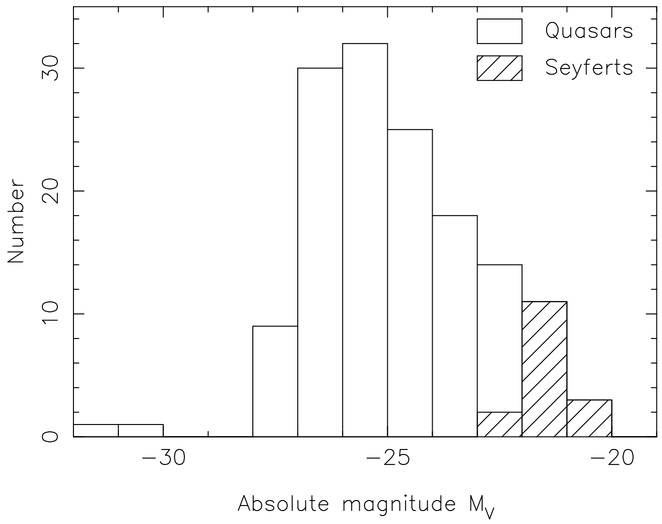

Figure 4.3: The distribution of absolute magnitudes for sources in the PHFS with quasi-simultaneous photometry. In calculating M_V, we used $H_0 = 75$ km s^{-1} Mpc^{-1} and $q_0 = 0.5$, and the spectral index α was calculated from the optical photometry. The open histogram shows those sources of quasar luminosity, while the hatched histogram shows those with Seyfert luminosity (see text for definition).

between the two classes is largely an arbitrary one (although we also note that even the low-redshift sources here are not true Seyferts, due to their strong radio emission – Seyfert galaxies are not generally radio-loud objects).

4.5 Errors

When the observational data was published (Francis et al. 2000), the quoted error for each object was the sum (in quadrature) of random errors (determined from the root-mean-squared pixel-to-pixel variation in the sky regions) and an assumed 5% systematic error in the photometric zero points (determined from the scatter in the zero points from different standard star measurements over the course of a night). The rms scatter in the zero points was typically $\leq 3\%$, so a somewhat conservative value of 5% was adopted as the systematic value.

However, for the purposes of the modelling to be done in this thesis, there are a number of potential systematic errors not considered in Francis et al. (2000) that may be important. These include:

① The optical zero magnitude fluxes (Bessell et al. 1998) were derived for an A0 star, and so will be slightly incorrect for a quasar spectrum. This has the effect of introducing small colour terms into the photometry, the size of which will depend on the spectral index of the object being observed. A similar effect will of course be present in the NIR. Bersanelli et al. (1991) found that spectral shape differences could produce systematic errors of at least a few percent in the NIR flux.

② The zero point fluxes in the optical and the NIR are taken from different references (see above). These different zero points may not be exactly equivalent, which will produce small offsets between the optical and NIR parts of the SED.

③ If the sky conditions at Siding Spring Observatory were not completely photometric for all observations for a given source (particularly if the transparency changed between different bands), then the measured photometry will have small band-to-band errors present.

④ The observations for each source were taken quasi-simultaneously (indicating all observations were made within at most a six-day period), to minimise the effects of variability. However, as discussed above, a number of the sources in the PHFS have been found to exhibit intraday variability in the optical (Heidt and Wagner 1996; Romero et al. 1999), and a larger number no doubt have similar properties to these. Therefore, variability on timescales of the order of those separating our observations is likely for some of the sources. Such variability can be up to 0.1 mag over the period of a night.

A possible example of a source that has undergone variability between the two sets of observations is the BL Lac 0537−441. This source has been shown to be quite variable on very short timescales (amplitudes of $\sim$ 0.3 mag on timescales of 2 days were seen by Romero et al. (2000)). Its SED is shown in Fig. 4.4, where it appears as if the NIR emission (which was observed after the optical) has been boosted – note that the slope of the NIR is approximately that of the optical (excluding the B band point), but with a different normalisation. This difference corresponds to a variation of $\sim$ 0.5 mag over the course of 4–5 nights. For further examples (although not as extreme) of such

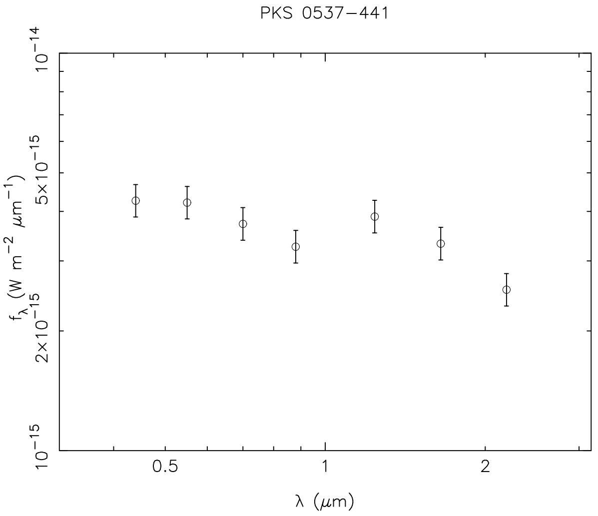

Figure 4.4: The SED of the BL Lac object 0537−441. Note that the three NIR points appear to be displaced upwards from the extrapolation of the optical points. Error bars are 1σ.

"micro-variability", see Chapter 8.

⑤ Finally, the presence of strong emission lines in the quasars' spectra could boost the flux of a band above the level of the continuum. The amount of this effect is investigated for a small number of objects in Section 5.9.

To account for all these extra effects, which will be present in all the objects in different amounts, we have increased the systematic error from 5% to 10%, while leaving the random error the same. These updated errors are shown in the tables of photometry (Tables B.1 & B.2).

4.6 Sources used

For the purposes of the modelling done in this thesis, not all of the sources that were observed will be used. The sources that are not are excluded for a number of reasons.

Firstly, we have excluded those sources that were not observed or detected in at least six bands. The reasoning behind this was to make sure that there were more points than free parameters in the model fitting (i.e. that the number of degrees of freedom in the fitting is significantly more

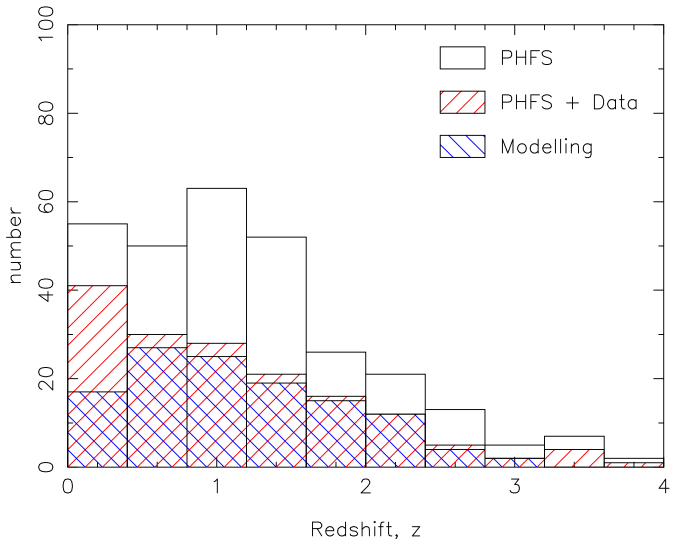

Figure 4.5: Redshift distribution, showing sources with photometry ("PHFS + Data") and those sources selected for modelling ("Modelling") (see text for criteria). The entire PHFS sample is shown for comparison ("PHFS").

than zero).

Secondly, sources without a measured redshift were excluded. The redshift is needed to accurately obtain the observed shape of the model (in particular those parts that are not a power law). Also, it is preferable to be able to use rest-frame quantities (such as wavelength), as these are intrinsic to the source and not dependent on the observer. One source that had an unknown redshift in Drinkwater et al. (1997), PKS 0829+046, has a published redshift of $z = 0.18$ (Falomo 1991) (found by fitting to the host galaxy emission), which is used herein.

Finally, also excluded from the main analysis were those sources with prominent additional spectral components. One class of these objects were the low-redshift galaxies, which show a prominent 4000Å break between the B and V bands. These sources show strong evidence for significant flux from the underlying galaxy in their spectra (Masci, Webster, and Francis 1998), and thus would need an additional galaxian component to be modelled accurately – this is beyond the scope of this thesis. The other class of sources to be excluded were the high-redshift (i.e. $z > 3$) quasars. These sources have strong Lyα breaks present between the B and V bands.

Once all these exclusions were made, the number of sources decreased from 157 to 117. For completeness, the redshift distribution of the selected sources, compared to that of the PHFS as a whole, and the sources with any optical/NIR photometry from Francis et al. (2000), is shown in Fig. 4.5. Note the large number of sources with small redshift that have been excluded (due to the criterion for removing galaxy-dominated sources). The only source with $z < 0.1$ is the BL Lac 1514−241 ($z = 0.0486$) – this source is dominated by its smooth continuum, so that no 4000Å break from the host galaxy is visible. The next highest redshift source is 0829+046 at $z = 0.18$. The photometry is listed in Table B.1, with the new errors, while the photometry for the excluded sources is listed in Table B.2, together with the reason for each source's exclusion.